A study on the homogeneous nucleation kinetics of model charged sphere suspensions

2002 J. Phys.: Condens. Matter 14 11573

(http://iopscience.iop.org/0953-8984/14/45/302)

INSTITUTE OF PHYSICS PUBLISHING JOURNAL OF PHYSICS: CONDENSED MATTER

J. Phys.: Condens. Matter **14** (2002) 11573–11587 PII: S0953-8984(02)52780-6

A study on the homogeneous nucleation kinetics of model charged sphere suspensions

Hans Joachim Schöpe and Thomas Palberg

Institut für Physik, Universität Mainz, Staudinger Weg 7, D-55099 Mainz, Germany

Received 9 September 2002
Published 1 November 2002
Online at stacks.iop.org/JPhysCM/14/11573

Abstract

We investigated the kinetics of homogeneous nucleation from a shear melt for a model system of deionized aqueous suspensions of charged spheres. With the aid of nearly index-matched perfluorinated particles of low polydispersity, we extended previous studies into the regime of large metastability and nucleation-dominated solidification. With increasing particle number density n, the solidification time determined by the appearance of a finite shear modulus decreased from minutes to milliseconds. Nucleation rate densities J were derived from the width of the principal peak in the static structure factor as measured by means of light scattering after complete solidification. J was observed to increase approximately exponentially with n as expected from classical nucleation theory in the absence of a kinetic glass transition. Additional measurements of the elastic and dynamic behaviour, however, show that for the largest concentrations, the sample properties are glass-like.

1. Introduction

The kinetics of the first-order freezing transition from the liquid to the solid state is a long-standing problem of great practical interest. Still we are lacking a comprehensive understanding and theoretical modelling of the nucleation and growth of crystals from a metastable melt. Investigations comprise theoretical and experimental approaches as well as computer simulations. In recent years, the study of experimental model systems in general and colloidal suspensions in particular has attracted considerable interest. Nucleation and growth [1–13] as well as vitrification [14–19] were experimentally studied by various optical methods, allowing convenient access both on the level of crystallites and on that of individual particles. At the same time, both theory and computer simulation drew on the analytically tractable interaction potential and provided valuable complementary approaches [20–24]. Considerable progress was made this way on nucleation and the glass transition of hard-sphere (HS) systems as well as on the growth of charged sphere (CS) systems.

One of the most important results was the confirmation of classical rate equation theories of nucleation for the case of HS suspensions [2, 4]. Classical nucleation theory states that

the kinetics is controlled by an exponential dependence on the ratio between some intrinsic energy scale and the thermal energy k_BT. From this, the nucleation rate density J is given as $J = J_0 \exp(-\Delta G^*/k_BT)$ [25, 26], where for colloidal systems the nucleation barrier $\Delta G^* = 16\pi\gamma^3/3(\Delta\mu\, n)^2$. Here $n = \Phi/(4\pi/3)a^3$ is the particle number density, with a being the particle radius and Φ the packing fraction; γ is the surface tension between the melt and the solid, which for HSs is of the order of k_BT/a^2. The kinetic prefactor for nucleation in colloidal systems reads $J_0 = nD_S^L/l^2$. The characteristic length scale l was approximated successfully by $l = d_{NN} \approx n^{-1/3}$ which leads to a $\Phi^{5/3}$ dependence of J_0 for HSs. J_0 further depends on the long-time self-diffusion coefficient D_S^L. Since D_S^L approaches zero at the HS glass transition, HS nucleation rates show a pronounced maximum [2, 4].

The corresponding rate equation theory of growth was proposed by Wilson and Frenkel [27] and was observed to apply for CSs [7, 8, 12]. The theory predicts the growth velocity to be $v = v_\infty[1 - \exp(-\Delta\mu/k_BT)]$, where $v_\infty = D_S^L d_I/l^2$ is the limiting velocity for infinite $\Delta\mu$ [4, 12]. For CS melts, D_S^L was measured close to freezing to be $D_S^L = 0.1D_0$ in agreement with simulation and theoretical calculations [21, 28, 29]. A second length scale is involved in growth: d_I is the thickness of the interfacial region between melt and solid. It was observed to be of the order of 2–6 d_{NN} for CSs, and in simulations on Lennard-Jones particles too [12, 30].

Nucleation data on CSs are still rare. A quantitative comparison to classical nucleation theory is still lacking, although an exponential decrease of crystallite sizes with increasing metastability has recently been reported by several authors [10, 13, 31]. One obvious reason for this is the more complex nature of the particle interaction. In CSs the interaction potential may be experimentally adjusted via the particle density and/or particle charge and/or concentration of the screening electrolyte. In turn also, the chemical potential difference $\Delta\mu$ depends sensitively on these parameters and, for each given sample, $\Delta\mu$ has to be determined experimentally or via computer simulation [12, 32]. The other reason is twofold and of experimental nature. Only close to the fluid–solid phase boundary is nucleation slow enough for direct video-microscopy [8, 11, 31]. Even time-resolved scattering experiment measurements become exceedingly difficult. At larger particle concentration, only an evaluation of crystallite sizes in completely solidified samples can be performed. Here either microscopy or static light scattering is employed. A severe limitation on such optical investigations is imposed by the onset of multiple scattering. At elevated particle concentrations, the generally water-based CS samples become too turbid for any further investigation.

A pioneering study was, however, reported by Beck *et al* [19] using static and dynamic light scattering on a charged sample comprising perfluorinated particles. Their index of refraction was close to that of the aqueous solvent, thus drastically increasing the sample transparency. While the strongly polydisperse sample showed crystallization at very low concentration, glass formation was observed at packing fractions around $\Phi \approx 0.15$ as characterized by the presence of a finite shear modulus and a 'frozen' short-range order. This is in line with two recent simulation studies which on one hand show that polydispersity may significantly suppress nucleation [24] and on the other hand predict a CS glass in that range of packing fractions, if the particle charge is sufficiently large [22].

The samples for the present study were selected to be monodisperse and carry a relatively small charge [33]. If fully deionized, they crystallize at low packing fractions of $\Phi \approx 0.001$, but the glass transition is expected to occur at much larger packing fraction than in [19]. Like these authors, we shall, however, exploit the optical properties of perfluorinated particles to study the homogeneous nucleation behaviour of fully deionized samples up to particle number densities of $n = 47.5\ \mu\mathrm{m}^{-3}$ corresponding to $\Phi \approx 0.15$.

Measurements of nucleation kinetics are accompanied by further experiments on phase behaviour, elasticity and diffusion to characterize the samples after crystallization. In this way

we are for the first time able to point out correlations between the concentration-dependent nucleation behaviour and the properties of the corresponding colloidal solids. In particular, we argue by comparison to the HS case that a kinetic glass transition is absent in our samples. Nevertheless, the supplementary data clearly indicate that at the largest concentration our system is essentially a glass.

In what follows we shall briefly introduce our model systems and sketch the techniques employed. We then describe our results and compute the nucleation rate densities. Finally, we will compare our findings with expectations from classical nucleation theory and also with the behaviour observed in HS model systems.

2. Experimental details

The multi-purpose light scattering experiment used in this study was recently described in detail elsewhere [34]. Static and dynamic light scattering which probe the structure and morphology of colloidal solids and their dynamics, respectively, are combined with torsional resonance spectroscopy to determine the shear modulus G. The most important feature of the method for the present study is the possibility to perform these experiments quasi-simultaneously on each individual sample, i.e. without the need to transfer the fragile samples from one set-up to another.

Optical studies without significant multiple scattering were facilitated using perfluoroethylene particles of density $\rho \approx 1.95$ g cm^{-3} and refractive index $\nu = 1.37$, close to that of water. The particles were a kind gift of Clariant, Gendorf, Germany (LOT# TF 9201E). The stock suspension of approximately 20% w/w was diluted with either water (sample series I) or water and glycerol to produce 40% w/w solvent mixtures (sample series II). The actual particle concentration was inferred for each sample from the positions of the Bragg reflections. Reliable results for static light scattering could be obtained up to particle number densities of $n = 35$ and 47.5 μm^{-3} for samples I and II, respectively. For larger concentrations, multiple scattering dominates. The hydrodynamic particle radius was determined by means of dynamic light scattering to be $a = 90$ nm. Two different measurements were employed to characterize the effective particle charge. Conductivity yields the packing-fraction-independent, small-ion-averaged effective charge via the measurement of the number of fully mobile counter-ions [33, 35]. It therefore accounts for counter-ion condensation under conditions of overlapping double layers. Effective charges from elasticity measurements depend on the evaluation of the shear modulus in terms of a screened Coulomb interaction. They thus implicitly also account for many-body forces through a further lowering of the effective charge [33, 34, 36]. The effective charges from conductivity are $Z^*_\sigma = 520 \pm 50$ and from elasticity $Z^*_G = 350 \pm 20$ (355 ± 20) for the water (glycerol/water) system (for details, see below). Comparison to other particle species of similar size and to charge renormalization theory shows that PTFE180 carries a relatively low effective charge [33]. This has two consequences. On the one hand we do not expect a kinetic glass transition in the concentration regime investigated. On the other hand PTFE180 is not fully stable against shear coagulation. Therefore, samples were deionized by introducing ion exchange resin (IEX, Amberlite UP 604, Rohm&Haas, Chancy, F) into the sample cell and occasional gentle shaking, thereby shear melting the sample. The residual ion concentration reached in this way was estimated from the conductivity to be of the order of 5×10^{-7} mol l^{-1}.

2.1. Static light scattering and phase behaviour

Under deionized conditions and at low particle number densities, samples of both series are fluid. Between $n_F = 2.7 \pm 0.2$ μm^{-3} and $n_M = 3.1 \pm 0.2$ μm^{-3} fluid and crystals coexist and

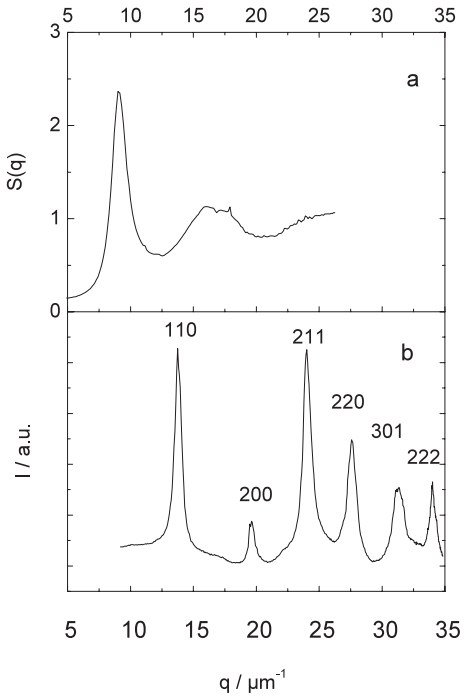

Figure 1. (a) The static structure factor of sample I (PTFE180 in water) measured under deionized conditions and for $n = 2.5\ \mu\mathrm{m}^{-3}$. (b) The scattered intensity $I(q)$ for sample I corrected for changes in the sampling volume measured under deionized conditions and at $n = 7\ \mu\mathrm{m}^{-3}$. Data were taken immediately after complete resolidification, as checked via the appearance of a finite shear modulus G'. The sample structure is bcc.

above the melting concentration samples are fully crystalline. Figures 1 and 2 give examples of static light scattering results obtained for different n-values for both series. The shift of q-ranges was accomplished by changing the wavelength. For the fluid sample the static structure factor is shown; it was calculated from a weighted division of the measured intensity at finite concentration by that measured without structure on a strongly diluted sample. Measurements were made on the crystalline sample at several different wavelengths. Furthermore, the inhomogeneous morphology of the grains plus grain boundary was observed to result in an ill defined additional incoherent background contribution. We therefore did not calculate the structure factor but rather show scattering intensities in arbitrary units. Note, however, that this affects neither the structure determination nor the determination of the peak widths.

For large n, further structure determination was performed via measurements of the shear modulus G using torsional resonance spectroscopy. The results are compiled in figure 3. With increasing n, the shear modulus is observed to increase by more than an order of magnitude from less than 1 Pa at the phase boundary to some 15 Pa at the largest accessible n. The low-n data are well described by the theoretical prediction for a body-centred cubic (bcc) polycrystalline solid using a morphology factor of $f_A = 0.5$. This factor results from the boundary conditions used in averaging over different crystal orientations; $f_A = 0.4$ for homogeneously distributed strains (grain boundaries perpendicular to the shear plane) and $f_A = 0.6$ for homogeneously distributed stresses (grain boundaries parallel to the shear plane or vitreous materials), in most polycrystalline materials; however, the ideal situations are not met and one observes $f_A = 0.5$ [37–40]. The residual impurity concentration is set to $c = 5 \times 10^{-7}$ mol l^{-1} as obtained from

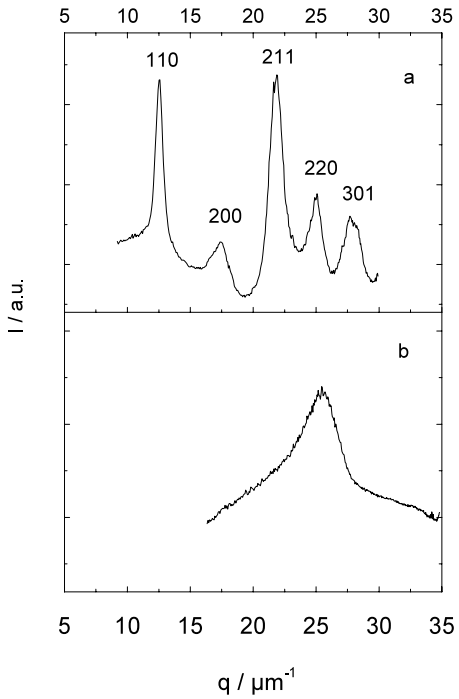

Figure 2. The scattered intensity $I(q)$ corrected for changes in the sampling volume for sample II (PTFE180 in a 40% w/w mixture of water and glycerol) measured under deionized conditions and for (a) $n = 5.7\ \mu\mathrm{m}^{-3}$ and (b) $47.5\ \mu\mathrm{m}^{-3}$. Both measurements were made immediately after complete resolidification as checked via the appearance of a finite shear modulus G'. The sample structure in (a) is again bcc.

the conductivity and an effective charge of $Z_G^* = 350 \pm 20\,(355 \pm 20)$ for sample I (sample II) is used as the only free parameter. At the largest concentrations, the data points lie higher than expected and are much better described by $f_A = 0.6$, if all other parameters are kept constant. This value of f_A corresponds to the limit of homogeneously distributed stresses and inhomogeneously distributed strains as expected for vanishing grain size and/or increasing amount of grain boundary material.

The good agreement with the theoretical expectation over the complete range of concentrations investigated clearly indicates that the sample structure stays bcc. The transition to a face-centred cubic (fcc) structure would result in a decrease of G as has been shown recently for a polystyrene sample of similar size [41]. The theoretically expected transition to the fcc state is either absent or pre-empted by the rapid solidification of the melt into the bcc structure which in that case would appear to be metastable [42, 43].

We may now compare the observed freezing and melting point transitions to the freezing line as determined from computer simulation. Following Robbins *et al* [20], figure 4 shows a plot of the ratio between thermal energy and pair interaction energy $k_BT/V(d_{NN})$ versus the coupling parameter $\lambda = \kappa d_{NN}$. Here κ is the Debye screening parameter and d_{NN} the nearest-neighbour distance. The symbols denote the pathway of the sample in this plot (the state line) as calculated using Z_G^* and particle number densities increasing from $n = 0.1\ \mu\mathrm{m}^{-3}$ (top) to $100\ \mu\mathrm{m}^{-3}$ (bottom left) [44]. Note that the interaction energy first increases rapidly, then more slowly, while the coupling first decreases, then increases. Large symbols correspond to the freezing transition. The lines give the results of two predictions for the freezing

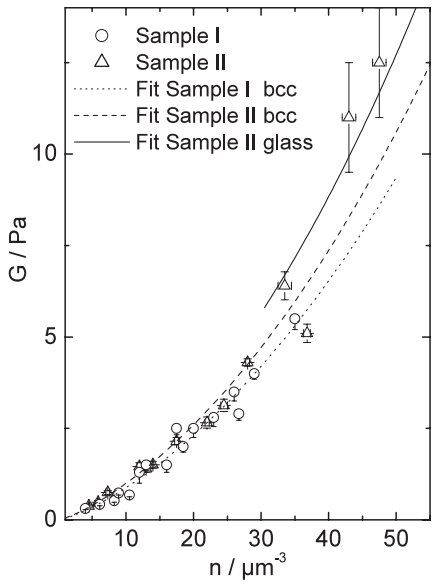

Figure 3. Static shear modulus G versus particle number density n. Circles: sample I; triangles: sample II. Solid, dashed and dotted curves are fits assuming bcc local order and different morphological factors (see the text for details).

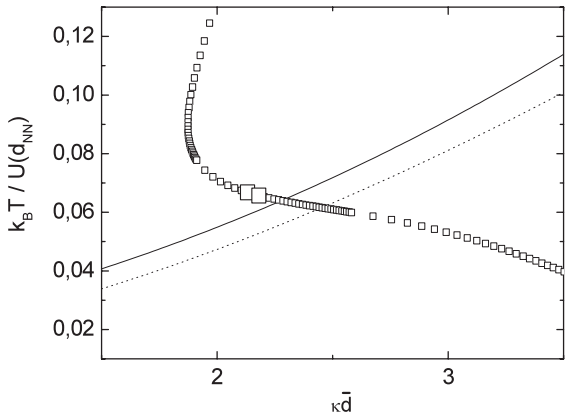

Figure 4. The universal phase diagram after Robbins *et al* [20] showing the reduced temperature–coupling strength plane. Symbols denote the pathway of our samples in this plane (the state line) upon increasing the particle number density from $n = 0$, 1 μm^{-3} (top) to 100 μm^{-3} (bottom left). These were calculated using Z_G^* and a residual ion concentration of $c = 5 \times 10^{-7}$ mol l^{-1}. For clarity, only data for sample series I are shown. Data for sample II are practically indistinguishable. The large symbols denote the experimental n_F and n_M, respectively. Solid and dotted curves correspond to the predictions for the freezing line from computer simulations by Robbins *et al* [20] and Meijer and Frenkel [45], respectively.

lines from computer simulations [20, 45]. The agreement achieved using the shear modulus charge is satisfactory and much better than that obtainable from the conductivity charge [46]. For the purposes of the present paper, we simply note that Z_G^* which corresponds to the ion- and particle-averaged effective interaction yields consistency between phase behaviour and elasticity.

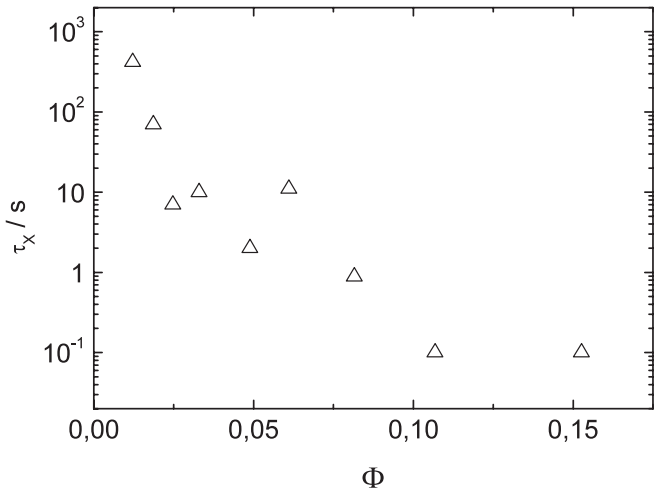

Figure 5. Solidification times versus packing fraction for sample II as determined from the appearance of a finite shear modulus. The solidification times decrease monotonically by more than three orders of magnitude.

2.2. Particle concentration dependence of the nucleation kinetics

In both sample series the times needed for complete solidification decreased drastically with increasing particle density n. Figure 5 shows the solidification times τ_X of sample series II determined via the appearance of a finite G. τ_X decreases monotonically by more than three orders of magnitude in the range of particle concentrations investigated.

At the same time, visual inspection reveals a rapid decrease of crystallite size with increasing n. This is also mirrored in the SLS patterns (cf figures 1 and 2). With increasing n we observe a pronounced broadening of the principal peak. From the full width at half-height Δq, the crystallite sizes L were computed using

$$L = 2\pi K/\Delta q \tag{1}$$

where the Scherrer constant for cubic crystals is $K = 1.155$ [2, 7]. Figure 6 compares the resulting L for the two samples. With increasing n or packing fraction $\Phi = 4\pi/3a^3n$, the crystallite size L decreases rapidly to values in the few-micron range.

Both data sets show some scatter at low concentration which is of statistical origin and due to the comparably small number of crystallites in the scattering volume which are oriented favourably for Bragg reflection. Data for sample series II taken around $n = 35\ \mu\text{m}^{-3}$ lie somewhat above the trend. The solvent mass density of sample series II is higher than for sample series I. It is further increased by the addition of the PTFE particles of mass density $\rho \approx 1.95\ \text{g cm}^{-3}$. At $\Phi \approx 0.11$ the ion exchange resin becomes buoyant and the somewhat larger crystals which usually form in the vicinity of the beads then occupy the scattering volume. At all other concentrations they are confined to either the cell bottom or top. This effect is, of course, absent for the water sample, where the ion exchange resin remains sedimented under all conditions.

At the largest concentrations investigated, a $(2.5 \times 2.5 \times 2.5)\ \mu\text{m}^3$ crystallite of sample II contains as few as $N \approx 750$ particles at $n = 47.5\ \mu\text{m}^{-3}$. We note that this is far fewer than in metallic nanocrystals [47, 48]. Very small crystallites were also observed for HSs close to the glass transition [2, 4, 15, 16]. Production of increasingly tiny crystals can be understood in terms of the Avrami scenario of nucleation and growth. In a series of papers, that author

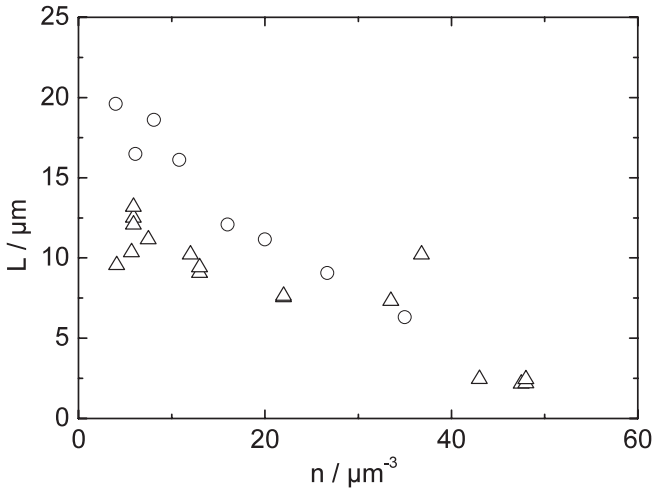

Figure 6. Crystallite sizes versus particle number density. Circles: sample series I; triangles: sample series II; crystallite sizes decrease with increasing n. The data for series II around $n = 35\ \mu\mathrm{m}^{-3}$ lie somewhat above the trend. This is attributed to the presence of ion exchange resin beads in the vicinity of the scattering volume. These become buoyant at this concentration in the glycerol/water sample, while the effect is absent in the pure water sample.

developed a model applicable in the case of constant nucleation rate densities J and constant growth velocities v which has since been applied to many atomic systems and also to colloidal suspensions [8, 49]. The model assumes non-interacting crystallites nucleating at random positions and growing undisturbed until their volume is equal to the sample volume. The resulting crystallite density is given by the simple expression

$$\rho = (\alpha J/v)^{3/4}. \tag{2}$$

Here $\alpha = 0.8636$ is a geometrical factor; $\rho = L^{-3}$ is the crystallite density as calculated by approximating the crystals as cubes of side length L. ρ depends on the ratio of nucleation to growth. Thus a few large crystallites will result for growth-dominated solidification and many small crystallites for nucleation-dominated solidification. The former is the case close to freezing at low metastability; the latter occurs at large metastability for both HSs and CSs. If both J and v are small, the solidification time τ_X will be large. This corresponds to the HS case, where both kinetic pre-factors scale with D_S^L and decrease to zero as the HS glass transition is approached. If on the other hand J and/or v are large, τ_X is short. This is the case for the PTFE180 system.

In the same theoretical framework the averaged steady-state nucleation rate densities J_{AVR} may be calculated from v and ρ. Rewriting equation (2) yields

$$J_{AVR} = 1.158 v \rho^{4/3} \tag{3}$$

where the subscript AVR discriminates from directly measured $J(t)$. The results are shown in figure 7 for both samples. J increases approximately exponentially and data points for sample II are systematically larger. At $n = 47.5$, nucleation rate densities above 10^{17} are reached.

The above evaluation may be criticized for several reasons. Before proceeding, we therefore briefly discuss these points. Firstly, since in the experimental system, growth is terminated by the intersection of crystallites, solidification is completed at larger times and the experimental crystallite density larger than expected in the model. Use of the model will thus

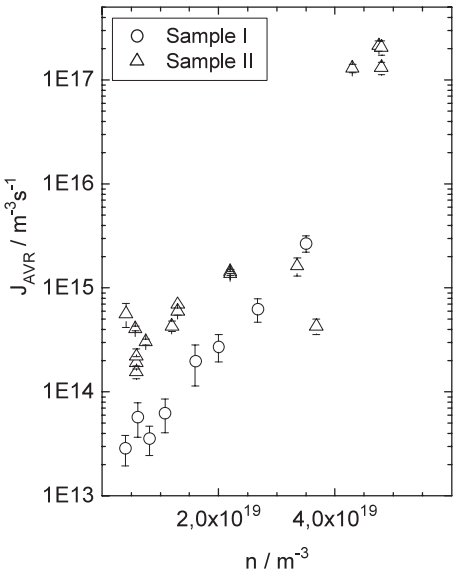

Figure 7. Steady-state nucleation rate densities as calculated from the crystallite sizes using equation (3) versus particle number densities. For both samples, J increases approximately exponentially.

lead to slight overestimation of J. We calculated the resulting error to be some 25% at low metastability and found it to further decrease with increasing metastability. This error thus appears to be smaller than the experimental uncertainty.

Of more importance is the correctness of the assumptions on the constancy of $J(t)$ and $v(t)$. A recent study on CSs in the growth-dominated regime has shown that close to the freezing transition the time-dependent nucleation rate density $J(t)$ may be peaked; i.e. after some short induction period, J increased strongly but decreased again towards zero before the sample was fully crystallized. Nevertheless, peak values of J and those determined from the Avrami model converged as the solidification scenario changed from growth to nucleation dominated [31]. As our investigations are mainly performed at large metastability, our samples are clearly in the nucleation-dominated regime.

Previous studies on the solidification of CS suspensions in the bcc region reported a linear increase of the extent of crystallites for both heterogeneously nucleated wall crystals and homogeneously nucleated bulk crystals, i.e. $v(t) =$ constant. Slightly larger values were reported for the bulk case as compared to the growth of oriented wall-based crystals [8, 12, 51]. For PTFE180, no growth data are available as yet. We therefore approximated the long-time self-diffusion coefficient as $D_S^L = 0.1D_0$ to obtain $v = v_\infty = 0.1D_0/d_{NN}$. This approximation was experimentally confirmed for samples at small to moderate metastability and also by computer simulation and theory [7, 28, 29]. At freezing, a value of $v = 3.5\ \mu\text{m s}^{-1}$ results, which was obtained at all concentrations.

The constancy of $v(n)$ will certainly not hold if a glass transition is encountered. This may, however, be checked. At the glass transition, both v and J would significantly decrease and this would lead to a drastic slowing of solidification. Referring to figure 5, we see that this is not the case for PTFE180.

A decrease of v is also expected from the influence of hydrodynamic interactions on the self-diffusion of particles. For HSs with their preferred position at contact, this effect is quite

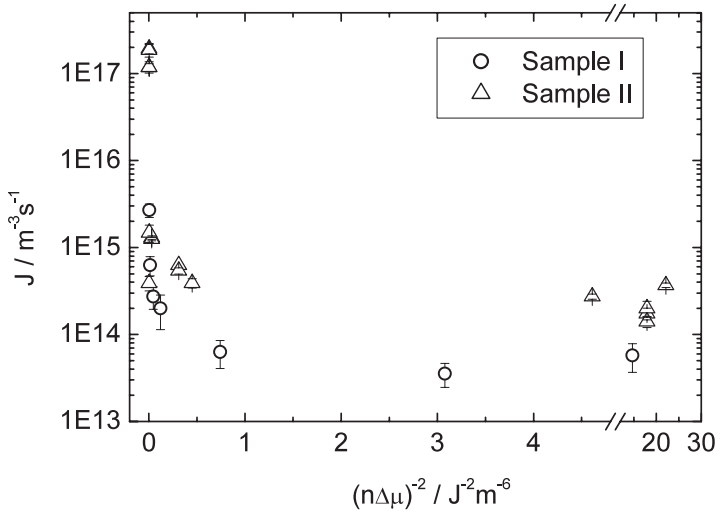

Figure 8. Nucleation rate densities versus $1/(n\,\Delta\mu)^2$. The key is as before. At low supersaturation, the nucleation rate densities are roughly constant at values of $J \approx 5\times10^{13}$ m^{-3} s^{-1} (5×10^{14} m^{-3} s^{-1}) for sample I (sample II). With increasing supersaturation, J increases drastically. The curves obtained cannot be described with a linear function.

large. For CSs, however, it is much weaker due to the electrostatic 'centring' of particles in their nearest-neighbour cage, which reduces the influence of hydrodynamic interactions [21, 50]. Using equation (3) and too large an estimate of v, the calculated J would be too large. Within experimental uncertainties on both Δq and τ_X, we estimate the maximum uncertainty in J to be a factor of two. This is too small to introduce a noticeable curvature in figure 7.

With these points clarified, we proceed to a qualitative comparison to classical nucleation theory. This in principle requires the knowledge of $\Delta\mu$. For PTFE180, neither experimental data nor computer simulations are available as yet. We follow Aastuen *et al* [51] and use the approximation $\Delta\mu = Bk_BT(n - n_F)/n_F$. For convenience, the proportionality constant B is set to $B = 10$, which is close to the value found by Aastuen *et al*. Würth *et al*, who investigated the growth of CS crystals, proposed an improved estimate relating $\Delta\mu$ to a rescaled energy density $\Pi^* = (\Pi - \Pi_F)/\Pi_F$. Here $\Pi = \alpha n V(d_{NN})$ with α being the particle coordination number. This approach considers both the direct density dependence and that of the pair interaction potential $V(r)$. In fact, large qualitative differences between the approach of Aastuen *et al* employed here and the improved version are found for highly charged particles. For these, $V(r)$ decreases past melting due to self-screening [44]. As can be seen from figure 4, this is not the case for PTFE180. In the absence of growth data, we therefore use the Aastuen *et al* estimate. In figure 8 we plot the nucleation rate densities versus $1/(n\,\Delta\mu)^2$. A straight line is expected for constant surface tension.

At low n and $\Delta\mu$, the data scatter about a constant value of $J \approx 5\times10^{13}$ m^{-3} s^{-1} (5×10^{14} m^{-3} s^{-1}) for sample I (sample II). No slope can be obtained with any accuracy. For $1/(n\,\Delta\mu)^2$ decreasing below 5, the curves bend upward with increasing steepness. This is not compatible with a constant surface tension, but seems to indicate an increase of γ with increasing metastability.

A similar observation was made in a preliminary investigation on salt-concentration-dependent J conducted rather close to the phase boundary [31]. There the constant values were observed to be of the order of $J \approx 5\times10^6$ m^{-3} s^{-1} at $n = 5.4\times10^{18}$ m^{-3}. The effect was

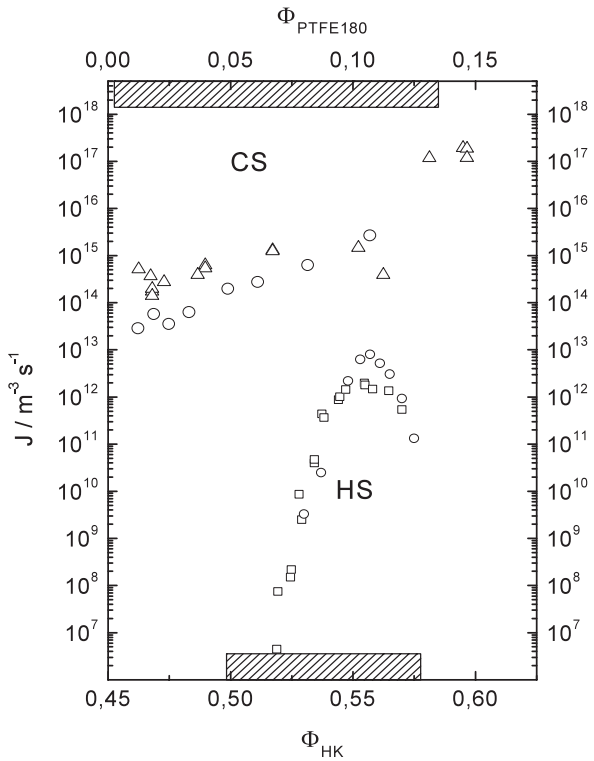

Figure 9. Calculated nucleation rate densities J versus packing fraction $\Phi = n(4\pi/3)a^3$. Upper scale and curves: PTFE180 (symbols as before); lower scale and curves: HS reference systems (squares: PMMA890 [5]; small circles: PMMA402 [2]). For HSs, J shows a maximum attributed to a decreasing diffusion constant in the melt. The hatched bars show the regions of visible crystallite formation. CS values are significantly larger than HS values and increase continuously over the range of packing fractions investigated. The density dependence is, however, less pronounced than in the HS case.

suspected to possibly originate from spurious impurity nucleation. Residual heterogeneous nucleation impurities may in principle be also present in this study, in particular since the ion exchange resin is present in the sample. We performed additional microscopic investigations to determine the concentration of visible contaminations (particle doublets, ion exchange resin splinters etc). It was found to be much too low to explain the observed J at small metastability. We therefore believe that for PTFE180 a density-dependent surface tension is the source of the observed behaviour.

We finally are concerned with a characterization of the resulting solids. Clearly, as the crystallite size is reduced, the sample morphology evolves from polycrystalline to nanocrystalline. A quantitative measure of this behaviour is given by the ratio $(q_{max}/\Delta q)^3 = (L/d_{NN})^3$ which gives the mass M of the crystallites. This is shown in figure 10.

The minimum values of M are compared to literature values in table 1. Fluids and liquids show values of $M \approx 100$–300, while for glasses $M \approx 300$–2000. Metal nanocrystals show values of M above 10^6. The influence of the nature of the interaction seems not significant. The present work yields 8000 for sample I and $M \approx 500$–600 for sample II. Interestingly, these values are much closer to the values obtained for vitreous systems than to those obtained for nanocrystals. Further, as shown in figure 3, the shear moduli for the most concentrated

Table 1. Compilation of experimental values for the number of particles per cluster in different systems of spherically symmetric interaction potential. HS: hard-sphere suspensions; CS: deionized charged sphere suspensions. (NC: nanocrystalline.) Values presented in the last column correspond to the largest particle number densities investigated in each sample series.

$M = (q_{max}/\Delta q)^3$						
Fluid CS [53–55]	Fluid HS [56, 57]	Liquid metal [53]	Glass CS [14, 19, 58]	Glass HS [19, 57, 59]	NC metal [47, 48]	Solid CS This work
2.3×10^2	$(1.6–2.3) \times 10^2$	1.2×10^2 (Rb)	$(1.8–2.4) \times 10^3$	6.8×10^2	$\geqslant 10^6$ (Al)	8×10^3 (I)
$(1.3–2.9) \times 10^2$	2.3×10^2	2.3×10^2 (K)	2.7×10^2	4.9×10^2	$\geqslant 3 \times 10^7$ (Fe)	$(5–6) \times 10^2$ (II)
$(1.6–2.2) \times 10^2$		85 (Cs)	7.3×10^2	5.7×10^2		

suspensions of sample II were much better described by a homogeneous distribution of stresses than one of strains. This is consistent with the expectation for amorphous materials or materials of very high defect concentration. Finally, we have also measured the dynamic behaviour by means of dynamic light scattering [34, 52]. For the most concentrated suspensions of sample II we observed a short time decay to a plateau value which is conventionally interpreted as 'rattling in the cage' of nearest neighbours. We were, however, not able to detect a second relaxation process on the experimental timescale. Such a behaviour was observed before in HS glasses and interpreted as suppression of structural rearrangements. Only on the timescale of months did the plateau shift to larger values. From this analysis of morphological, elastic and dynamic properties, we reach the conclusion that the solid formed from sample II at $n = 47\ \mu\mathrm{m}^{-3}$ is essentially a glass.

3. Discussion

The present investigation gave three major results. Firstly, the nucleation rate was observed to increase exponentially without any sign of interference of a kinetic glass transition. Secondly, the qualitative comparison to the expectations of classical nucleation theory indicated a density dependence of the surface tension. Thirdly, the samples showed polycrystalline-to-nanocrystalline morphology, but at the largest concentrations the resulting solids were observed to be glass-like. We shall address these results in the above order.

The observed exponential increase of J is similar to the HS case, if we restrict the comparison to packing fractions close to the phase boundary. This is shown in figure 9, which compares the PTFE180 data to those taken from two different HS reference samples [2, 5]. In all cases the range of packing fractions investigated spans some 15% and samples were investigated well into the nucleation-dominated regime. Note, however, that CSs were investigated at much lower absolute values.

For HSs at elevated packing fraction, the increased thermodynamic drive is overcompensated by the slowing of kinetic pre-factors as the glass transition is approached. Therefore J shows a maximum. This has been demonstrated by successful two-parameter fits of classical nucleation theory expressions yielding constant surface tensions of the order of $0.4–0.6\, k_B T/a^2$ in good agreement with theoretical expectations [2, 5, 7, 60, 61]. The kinetic slowing was also observed in theoretical calculations using a microscopic kinetic model [62]. It is absent in our monodisperse CS case, where solidification continuously accelerates with increasing n.

Nevertheless the exponential increase of J with n remains somewhat puzzling. As demonstrated both theoretically and in computer simulations, it is expected only if (like for

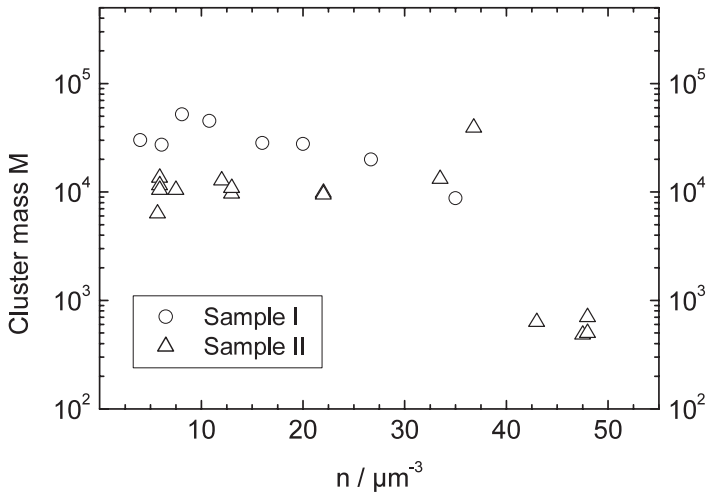

Figure 10. Cluster mass M as calculated from the ratio of peak width to peak position versus particle number density. Note that the smallest regions of correlated structure contain only some (5–7) $\times$ 10^2 particles. The transition from polycrystalline to nanocrystalline to glass-like appears to be continuous.

HSs) both the pair interaction and the surface tension are constant [8, 24, 63]. Then a linear decrease of the nucleation barrier $\Delta G^* = 16\pi\gamma^3/3(\Delta\mu\, n)^2$ and thus an exponential increase of J is found.

In our case the pair potential at the nearest-neighbour distance increases by some 30% over the range of n investigated (cf figure 4). Figure 8 further indicates a possible increase of surface tension with increased density. Therefore a strictly exponential increase in J is not expected. Either the measured range of n and the changes of $V(r)$ and γ are to small to result in noticeable deviations or we witness some cancellation of effects. Both cases call for further experimental studies facilitating quantitative comparisons to classical nucleation theory.

They also call for further theoretical investigations on systems more complex than monodisperse HSs. Here, some progress was reported very recently. Density-dependent surface tensions were observed in computer simulations by Auer and Frenkel for polydisperse HSs [24]. A polydispersity-induced change of γ with n may be the underlying reason for the observations of Beck *et al* [19], but should be of no concern here. In a second study the same authors, however, observed non-constant surface tensions also for the case of hard-core Yukawa spheres [64]. As a function of several suspension parameters, quite complex behaviour of γ was observed. To be specific, γ was found to increase with $\Delta\mu$ or Φ if the surface potential was increased at constant screening. If the potential was fixed, however, a non-monotonic dependence on κ was found, while the increase with $\Delta\mu$ or Φ, was retained. For each of their sample series, this resulted in an approximately linear decrease of ΔG^* with Φ. Unfortunately, fixing either the surface potential or the screening does not correspond to the experiment, where an increase of *n at the same time* alters both. Therefore, what the behaviour of J will be in a simulation that corresponds to the experiments remains an interesting open question.

We finally comment on the nature of the solids at largest concentrations. From our investigations it is clear that this state was reached via a drastic increase of nucleation rates. It has to be clearly discriminated from the conventional kinetic glass obtained in HS systems or polydisperse CS systems if nucleation is slowed and finally suppressed. Nevertheless, this state has a finite shear modulus, has a structural arrest on long timescales and long-range

order is absent. The last criterion possibly gives the best hint as regards how to distinguish the two versions of an amorphous state. In the HS case the local order is fluid-like; in the case of PTFE180 it is crystalline but interrupted at the cluster boundary. A second criterion may be the route taken into the amorphous state. In HSs, crystallization is suppressed; in the PTFE180 system, it is enhanced. We might summarize this as: 'nucleation supports vitrification'. More prosaically: if the nuclei intersect each other as soon as they are created, no long-range order may result. A sufficiently monodisperse and at the same time low-charge colloidal system seems to take a different route to a different amorphous state. Only at still larger packing fraction should the conventional kinetic glass transition also occur for PTFE180. This, however, was beyond the scope of the present paper.

Acknowledgments

It is a pleasure to thank W van Megen, P Leiderer, H Löwen, D Frenkel and K Binder for stimulating discussions, Clariant (FRG) for the kind gift of PTFE180 and W van Megen, A Heymann and A Stipp for the HS reference data. Financial support by the DFG (SFB262 TP20; Pa459/8,9) and the MWFZ, Mainz, is gratefully acknowledged.

References

[1] Bartlett P and van Megen W 1994 *Granular Matter* ed A Mehta (New York: Springer) p 195
[2] Harland J L and van Megen W 1996 *Phys. Rev.* E **55** 3054
[3] Russel W B, Chaikin P M, Zhu J, Meyer W V and Rogers R 1997 *Langmuir* **13** 3871
[4] Heymann A, Stipp A, Sinn Chr and Palberg T 1998 *J. Colloid Interface Sci.* **207** 119
[5] Stipp A, Heymann A, Sinn Chr and Palberg T 2001 *Prog. Colloid Polym. Sci.* **118** 266
[6] Gasser U, Weeks E, Schofield A, Pusey P N and Weitz D A 2001 *Science* **292** 258
[7] Palberg T 1999 *J. Phys.: Condens. Matter* **11** R323
[8] Aastuen D J W *et al* 1990 *Phase Transitions* **21** 139
[9] Dhont J K G, Smits C and Lekkerkerker H N W 1992 *J. Colloid Interface Sci.* **152** 386
[10] Okubo T 1994 *Macro-Ion Characterization: from Dilute Solution to Complex Fluids (ACS Symp. Ser. vol 548)* ed K S Schmitz (Washington, DC: American Chemical Society) p 364
[11] Grier D G and Murray C A 1994 *J. Chem. Phys.* **100** 9088
[12] Würth M, Schwarz J, Culis F, Leiderer P and Palberg T 1995 *Phys. Rev.* E **52** 6415–23
[13] Palberg T, Mönch W, Schwarz J and Leiderer P 1995 *J. Chem. Phys.* **102** 5082–7
[14] Sirota E B, Ou-Yang H D, Sinha S K, Chaikin P M, Axe J D and Fujii Y 1989 *Phys. Rev. Lett.* **62** 1524
[15] Pusey P N and van Megen W 1989 *Nature* **320** 340
[16] van Megen W 1995 *Transp. Theory Stat. Phys.* **24** 1017
[17] Härtl W, Versmold H and Zhang-Heider X 1995 *J. Chem. Phys.* **102** 6631
[18] van Megen W, Mortensen T C, Williams S R and Müller J 1998 *Phys. Rev.* E **58** 6073
[19] Beck Ch, Härtl W and Hempelmann R 1999 *J. Chem. Phys.* **111** 8209
[20] Robbins M O, Kremer K and Grest G S 1988 *J. Chem. Phys.* **88** 3286
[21] Banchio A J, Nägele G and Bergenholtz J 2000 *J. Chem. Phys.* **113** 3381
[22] Lai S K, Ma J W, van Megen W and Snook I K 1997 *Phys. Rev.* E **56** 766
[23] Cummins H Z, Li Gen, Hwang Y H, Shen G Q, Du W M, Hernandez J and Tao N J 1999 *Z. Phys.* B **103** 501
[24] Auer S and Frenkel D 2001 *Nature* **409** 1020
Auer S and Frenkel D 2001 *Nature* **413** 711
[25] Becker R and Döring W 1935 *Ann. Phys., NY* **24** 719
[26] Turnbull D and Fisher J C 1949 *J. Chem. Phys.* **17** 71
[27] Wilson H A 1900 *Phil. Mag.* **50** 238
Frenkel J 1933 *Z. Sowjetunion* **1** 498
[28] Löwen H, Simon R and Palberg T 1993 *Phys. Rev. Lett.* **70** 1557–61
[29] Bitzer F, Palberg T, Löwen H, Simon R and Leiderer P 1994 *Phys. Rev.* E **50** 2821–6
[30] Burke E, Broughton J Q and Gilmer G H 1988 *J. Chem. Phys.* **89** 1030
[31] Schöpe H J, Palberg T, Schwarz J and Leiderer P unpublished results

[32] Ripoll M S, Tejero C F and Baus M 1996 *Physica* A **234** 311–17
[33] Wette P, Schöpe H J and Palberg T 2002 *J. Chem. Phys.* **116** 10981–8
[34] Schöpe H-J and Palberg T 2001 *J. Colloid Interface Sci.* **233** 149
[35] Hessinger D, Evers M and Palberg T 2000 *Phys. Rev.* E **61** 5493–506
[36] Klein R, von Grünberg H H, Bechinger C, Brunner M and Lobashkin V 2002 *J. Phys.: Condens. Matter*
(Klein R, von Grünberg H H, Bechinger C, Brunner M and Lobashkin V 2002 Macroion shielding and state dependent pair potentials in colloidal suspensions *Preprint*)
[37] Schmid E and Boas W 1935 *Kristallplastizität* (Berlin: Springer)
[38] Hill R 1952 *Proc. Phys. Soc.* A **65** 349
[39] Hashin Z and Shtrikman S 1962 *J. Mech. Phys. Solids* **10** 343
[40] Zeller R and Dederichs P H 1973 *Phys. Status Solidi* b **55** 831
[41] Schöpe H-J, Decker Th and Palberg T 1998 *J. Chem. Phys.* **109** 10068–74
[42] Alexander S and McTague J P 1978 *Phys. Rev. Lett.* **41** 702
[43] Auer S and Frenkel D 2002 *J. Phys.: Condens. Matter*
Auer S and Frenkel D 2002 Numerical study of crystallization in charged colloids *Preprint*
[44] Liu J, Schöpe H J and Palberg T 2001 *J. Chem. Phys.* **116** 5901–7
[45] Meijer E J and Frenkel D 1991 *J. Chem. Phys.* **94** 2269
[46] Schöpe H J, Wette P and Liu J 2002 Consistency of the mean field description of charged colloidal crystal properties *Phys. Rev. Lett.* submitted
[47] Cullity B D 1978 *Elements of X-Ray Diffraction* (London: Addison-Wesley)
[48] Hammond C 1998 *The Basics of Crystallography and Diffraction* (Oxford: Oxford University Press)
[49] Avrami M 1939 *J. Chem. Phys.* **7** 1003
Avrami M 1940 *J. Chem. Phys.* **8** 212
Avrami M 1941 *J. Chem. Phys.* **9** 177
[50] Overbeck E, Sinn Chr and Watzlawek M 1999 *Phys. Rev.* E **60** 1936–9
[51] Aastuen D J W, Clark N A, Kotter L K and Ackerson B J 1986 *Phys. Rev. Lett.* **57** 1733
Aastuen D J W, Clark N A, Kotter L K and Ackerson B J 1986 *Phys. Rev. Lett.* **57** 2772 (erratum)
[52] Schöpe H-J and Palberg T 2001 *Prog. Colloid Polym. Sci.* **118** 82
[53] Cotter L K and Clark N A 1987 *J. Chem. Phys.* **86** 3646
[54] Härtl W and Versmold H 1988 *J. Chem. Phys.* **88** 7157
[55] Härtl W, Versmold H and Wittig U 1984 *Ber. Bunsenges. Phys. Chem.* **88** 1063
[56] Russel W B, Saville D A and Schowalter W R 1989 *Colloidal Dispersions* (Cambridge: Cambridge University Press)
[57] van Megen W, Underwood S M and Pusey P N 1991 *J. Chem. Soc. Faraday Trans.* **87** 395
[58] Härtl W, Versmold H and Zhang-Heider X 1995 *J. Chem. Phys.* **102** 6631
[59] Snook I, van Megen W and Pusey P N 1991 *Phys. Rev.* A **43** 6900
[60] Marr D W M 1995 *J. Chem. Phys.* **102** 8283
[61] Davidchack R L and Laird B B 2000 *Phys. Rev. Lett.* **85** 4751
[62] Dixit N M and Zukoski C M 2002 *Phys. Rev.* E **64** 041604
[63] Russel W B 1990 *Phase Transitions* **21** 127
[64] Auer S and Frenkel D 2002 *J. Phys.: Condens. Matter* **14** 7667